Copper-Modified TiO2 and ZrTiO4: Cu Oxidation State Evolution during Photocatalytic Hydrogen Production

Copper modified TiO_2 and $ZrTiO_4$: Cu oxidation state evolution during photocatalytic hydrogen production

Valeria Polliotto[1], Stefano Livraghi[1], Anna Krukowska[2], Maria Vittoria Dozzi[3], Adriana Zaleska-Medynska[2], Elena Selli[3] and Elio Giamello[1]*

[1]Dipartimento di Chimica and NIS, Università di Torino, Via P. Giuria 7, 10125 Torino, Italy.

[2]Department of Environmental Technology, Faculty of Chemistry, University of Gdansk, 80-308 Gdansk, Poland.

[3]Dipartimento di Chimica, Università degli Studi di Milano, Via Golgi 19, Milano, Italy

Keywords: copper, Cu_2O, Cu^{2+}, HER, EPR, TiO_2, $ZrTiO_4$

ABSTRACT

In the present work two H_2 evolution photocatalysts were prepared employing two different oxides, TiO_2 and zirconium titanate ($ZrTiO_4$), as support of the various copper phases. For both the supports the same Cu loading (0.5% w/w) was adopted, but two different impregnation procedures have been followed leading to different forms of Cu in the final composite material that are: i) Cu(II) species dispersed on the oxide surface; ii) Cu_2O particles dispersed on the oxide surface.

The present paper based on the parallel use of photocatalytic test and spectroscopic analysis performed in catalytic conditions illustrates the evolution of photocatalytic systems occurring during the H_2

evolution reaction tests, pointing out that the as prepared materials represent a pre-catalyst and they are modified during irradiation leading to the real working systems different from the starting ones.

The here presented spectroscopic analysis aims to contribute to the living debate on the oxidation state of copper in mixed Cu/oxide materials and on its role in hydrogen evolution under photocatalytic conditions.

1. INTRODUCTION

The increased demand of energy resources coupled with the necessity to face environmental pollution led to a growing interest in H_2 production.[1] Among the possible strategies to produce H_2, both water photo-splitting and photo-reforming of small hydrocarbons are attracting a continuously growing interest. Up to date, several different materials have been proposed as candidates for these applications.[2] Among the possible materials suitable for photocatalytic applications, titanium dioxide still remains the most investigated one, mainly because of its peculiar physical and chemical properties.[3] In spite of the great potential of this material in several photocatalytic applications, H_2 production does not efficiently proceed on titanium dioxide, at least in its bare form, mainly due to the rapid recombination of the photogenerated charge carriers and the insufficient reduction potential at the conduction band edge. To increase the rate of H_2 formation several strategies have been developed, e.g. by co-catalysts (Pt, Au …) addition or by coupling the solid with other semiconducting materials with suitable band potentials.[4-7]

The modification of semiconducting oxides with copper represents a strategy of great interest due to the remarkable H_2 evolution rates attained under irradiation and for the low cost of copper with respect to other co-catalysts such as platinum and gold. Nevertheless, up today, there is not a general consensus in the interpretation of the mechanism behind the relatively high efficiency of Cu/TiO_2. This is mainly due

to the capability of copper to easily attain different oxidation states and to the fact that the preparation pathway can affect the ratio among these different forms of Cu.

As far as the different forms of copper and the related activities are concerned, the following information can be drawn from the available literature.

a) Cu(II) species. The presence of cupric ions on the surface of Cu-modified oxides is indicated by some authors as the origin of the photoactivity of these materials under visible light. Such activity is ascribed to the charge transfer from the oxide valence band to the Cu^{2+} surface states, which in turn, generate Cu^{+} species capable of one-electron transfer to adsorbed species to some extent.[8,9] Concerning H_2 evolution, however, the surface sites and the involved mechanism are still under debate and conflicting models can be found in the literature. The sole presence of isolated Cu^{2+} ions, in fact, is not enough to explain the high activity of Cu(II) modified materials since the reduction potential for the Cu^{2+}/Cu^{+} redox couple is positive (0.16 V).[8] To overcome this contradiction, since CuO is reported to be active in the H_2 photoproduction,[10] it was proposed however that the decoration with Cu(II) ions of an oxide surface, such as TiO_2, can lead to the formation of CuO-like (CuO_x) structures.[11] Nevertheless, up today there is not a general consensus about the mechanism operating in presence of this oxide. Some authors in fact claim that CuO is not able, in principle, to photo-produce H_2 due to the unfavourable conduction band potential and fast recombination of the charge carriers,[12-15] It is also reported however that the surface impregnation procedure, usually adopted to prepare this kind of composite materials, can lead to the formation of a thin layer of CuO at the surface of the supporting oxide. This kind of layer, due to quantum size effects, should be characterized by a larger band gap than that of bulk CuO with the conduction band edge shifted to a more negative potential so enabling the enhancement of H_2 evolution rate.[16,17] Recently it has also been proposed that, during the photocatalytic process, the surface CuO_x species are converted in low oxidation forms of copper (Cu^{+})[18-20] and Cu_2O represents the real active species.[21,22]

b) Cu(I) species. Several studies have shown that the presence of cuprous oxide (Cu_2O) on the surface of materials such as TiO_2 or ZnO drastically enhances the H_2 evolution rate with respect to the bare material. Again Cu_2O is a semiconducting oxide (E_g 2.0-2.5 eV) but, differently from the case of cupric oxide, the high H_2 evolution rate, in this case, is unambiguously ascribed to the features of the formed oxide-oxide heterojunction. In this case, in fact, the band gap alignment of the two oxides improves the charge carriers separation and, consequently, the H_2 evolution capability.[19,21-24]

c) Metallic Cu. Copper nanoparticles supported on oxides were widely studied as catalysts for carbon monoxide oxidation and more recently, Surface Plasmon Resonance (SPR)-driven photocatalysis has been demonstrated in titania/copper systems under visible-light irradiation.[25] As far as H_2 photo-production is concerned some papers show that, in the presence of metallic Cu, the H_2 evolution rate increases suggesting that copper can act as a co-catalyst also this form, promoting H_2 evolution as in the case of other noble metals.[15,21,26-30] Some authors also report that during the H_2 photoformation process on Cu_2O modified materials the formation of metallic copper can occur.[23,24]

The present work is based on the joint use of Electron Paramagnetic Resonance (EPR) spectroscopy and UV-Visible Diffuse Reflectance Spectroscopy (DRS) to investigate the state and the role of copper compounds deposited (0.5% w/w) on two distinct semiconducting oxides. In the systems under investigation both Cu^{2+} ions ($3d^9$) and the paramagnetic centres, originated by the stabilization of photogenerated charge carriers in the supporting oxide, can be investigated by EPR spectroscopy. As to the other possible copper based species (Cu(I) and Cu(0)), these can be appropriately studied by optical spectroscopy (DRS) since they have specific absorption in the visible region.

Two different oxides were chosen as support of the various copper phases, namely TiO_2 and zirconium titanate ($ZrTiO_4$), in order to investigate the role of different oxidic supports on the charge carriers fate and H_2 evolution rate. The interest in zirconium titanate is due to its conduction band potential which is

slightly more negative than that of TiO_2, thus a higher reductive potential of photoexcited electrons is expected, making this material a possible candidate for hydrogen evolution via water photoreduction.

For the surface modification of the bare oxides with Cu, the same loading has been adopted for each sample (0.5% w/w), but two different impregnation procedures have been followed leading to different forms of copper in the final composite material that are: i) surface impregnation of the oxides with a $Cu(NO_3)_2$ solution. In this case the resulting starting material is essentially based on Cu(II) species dispersed on the oxide surface; ii) surface impregnation with pre-formed Cu_2O oxide.

The present paper illustrates the evolution of photocatalytic systems based on a semiconducting oxide (either TiO_2 or $ZrTiO_4$) modified at the surface, as described above, with copper containing species. It will be shown in the following that the starting materials (or pre-catalysts) undergo dramatic modifications during irradiation leading to working systems quite different from the starting ones.

The here presented spectroscopic analysis aims to contribute to the living debate on the oxidation state of copper in mixed Cu/oxide materials and on its role in hydrogen evolution under photocatalytic conditions.

2. EXPERIMENTAL

2.1. Samples preparation

The two oxide adopted as copper support (TiO_2 and $ZrTiO_4$) were prepared according to the Sol-Gel synthesis reported in previous works.[31,32] In a second step the modification with copper (0.5% w/w) was obtained via the two procedure below reported.

The Cu_2O-TiO_2 (hereafter Cu_2O-T) and Cu_2O-$ZrTiO_4$ (hereafter Cu_2O-ZT) powders were prepared by Cu(II) chemical reduction (via Benedict reaction) followed by a deposition procedure. To 10 ml of $Cu(NO_3)_2 \cdot 3H_2O$ water solution ($7.9 \cdot 10^{-3}$ M) 0.06 g of glucose and 15 ml of NaOH $2.4 \cdot 10^{-3}$ M were added. The solution was stirred for 50 min at 343 K. At the end of the reaction, a red suspension was

formed (suspension A). In this step of the preparation procedure, the glucose reduces the Cu^{2+} ions to Cu^{+} ions and the corresponding oxide (Cu_2O) is formed. 1 g of oxide (TiO_2 or $ZrTiO_4$) was suspended in 20 ml of deionized water and the suspension was sonicated at 333 K for 10 min (suspension B). Suspension A was added to suspension B and stirred for 10 min at 343 K. The so obtained pale pink powder was filtered and washed three times with water and ethanol in order to remove the reaction residues and finally dried at 343 K.

The Cu^{2+}-TiO_2 (hereafter Cu^{2+}-T) and Cu^{2+}-$ZrTiO_4$ (hereafter Cu^{2+}-ZT) powders were prepared by the wet impregnation method. 1 g of oxide (TiO_2 or $ZrTiO_4$) was suspended in 20 ml of deionized water and the suspension was sonicated at 333 K for 10 min. 10 ml of $Cu(NO_3)_2 \cdot 3H_2O$ $7.9 \cdot 10^{-3}$ M were added to the oxide suspension and sonicated for 50 min at 333 K. The so obtained suspension was stirred at 353 K until the formation of a dried pale blue powder. The powder was calcined in air at 623 K for 4 h and then washed three times with water.

Summarizing, since the copper loading was kept constant in all cases we investigated in this work four different systems, namely Cu^{2+}/T, Cu_2O/T (based on TiO_2) and Cu^{2+}/ZT, Cu_2O/ZT (based on $ZrTiO_4$).

2.2. Characterization methods

2.2.1. Characterization of the as prepared samples

The powder X-ray diffraction (XRD) pattern was recorded with a PANalytical PW3040/60 X'Pert PRO MPD diffractometer using a copper Kα radiation source. The diffraction patterns were obtained in the 2θ range between 20° and 80°. The X'Pert High-Score software was used for data handling.

The UV-Visible Diffuse Reflectance (DR-UV-Vis) spectra of the prepared solid were recorded using a Varian Cary 5000 spectrometer. A Polytetrafluoroethylene (PTFE) sample was used as the reference. The spectra were recorded in the 200–800 nm range at a scan rate of 240 nm/min with a step size of 1 nm. The measured reflectance was converted with the Kubelka-Munk function.

The specific surface area was measured with a Micromeritics ASAP 2020 apparatus using the Brunauer–Emmett–Teller (BET) model for N_2 adsorption measurements. Prior to N_2 adsorption, the sample was outgassed at 573 K for 2 h.

Continuous Wave Electron Paramagnetic Resonance (CW-EPR) experiments were performed with a Bruker EMX spectrometer operating at X-band (9.5 GHz), equipped with a cylindrical cavity operating at 100 kHz field modulation. All the spectra were recorded in vacuum condition at 77 K in a EPR cell that can be connected to a conventional high-vacuum apparatus (residual pressure < 10^{-4} mbar). In all cases the parameters setup was Modulation Amplitude 0.2 mT and microwave power of 10 mW.

2.2.2. Photocatalytic test

The hydrogen evolution tests were performed in a 100 ml quartz reactor with a rubber septum for bubbling and sampling. 0.1 g of photocatalyst were suspended in a 10% v/v methanol aqueous solution (72 ml H_2O and 8 ml of methanol) and sonicated for 10 min. The irradiation source was a 150 W Hamamatsu L2274 Xe lamp with a UV irradiance of 400 W/m^2. A magnetic stirrer was placed at the bottom of the reactor to keep the particles in suspension during the experiment. Prior to illumination, nitrogen was purged into the reactor for 30 min to remove dissolved oxygen. The photocatalytic hydrogen activity was then studied by illuminating the suspension for 4 hours. To evaluate hydrogen generation, a 200 µl gas sample was taken every 30 min from the reactor head space through a rubber septum. The gas samples were then injected into a Perkin Elmer Clarus 500 gas chromatograph (GC) equipped with HayeSep Q (80/100) column and thermal conductivity detector (TCD). Nitrogen was used as the GC carrier gas, at a flow rate of 1.0 ml/min.

2.2.3. Characterization of irradiated materials

The EPR spectra of the powders upon irradiation and in vacuum condition were recorded in the EPR cavity illuminated by a 1600 W Newport Xe lamp (irradiance 300 W/m^2). The samples were kept at 77 K in liquid nitrogen.

The EPR spectra characterization along the H_2 evolution process were obtained irradiating, with a 500 W Newport Hg-Xe lamp (irradiance 100 W/m^2) 10 mg of sample dispersed in 100 μL of water/methanol solution (10% v/v) in an EPR tube. Prior to illumination, the EPR cell was evacuated to remove O_2 while keeping the sample at low temperature in order to avoid the evaporation of the water/methanol solution.

The experiments were performed stepwise. After each irradiation step the sample was rapidly frozen from RT to 77 K and transferred in the EPR cavity to record the spectrum.

The parameters used for all the EPR spectra were Modulation Amplitude 0.2 mT and microwave power of 10 mW.

The DR-UV-Vis investigations during H_2 evolution process were performed irradiating with a 500 W Newport Hg-Xe lamp (irradiance 100 W/m^2) 0.4 g of samples suspended in 2 ml of water/methanol solution (10% v/v) in a quartz cell for DR-UV-Vis measurements. After irradiation, prior to the spectra acquisition the sample were let to sediment on the bottom of the cell. The DR-UV-Vis spectra were recorded in the 200–2500 nm range at a scan rate of 240 nm/min with a step size of 1 nm. Since the samples could not be stirred during irradiation, after every irradiation step the samples were sonicated in order to disperse the powders homogenously.

3. RESULTS AND DISCUSSION

3.1. Structural and optical characterization.

Fig. 1 reports the XRD and the UV-Visible DRS characterization of the two sets of Cu modified samples (T and ZT respectively) compared with the corresponding pristine materials. XRD diffractograms indicate that, for both oxidic supports (Fig. 1 A and B), the procedures adopted for the surface

modification with copper do not alter the crystallographic features of the oxides. Also the surface area is not affected by the two modification procedures (Table 1).

It is worth to note that the presence of the additional fraction of copper species can be detected by XRD in the case of the materials decorated with the Cu_2O particles only. Both Cu_2O-T and Cu_2O-ZT samples, indeed, show a very weak additional diffraction peak at about θ= 36.5° due to the (111) reflection of the Cu_2O lattice. This indicates that, even though the Cu loading adopted for the two surface modification procedures is the same (0.5% w/w), the surface distribution of the copper is different in the two kinds of materials. In the case of materials prepared via wet impregnation (Cu^{2+}-T and Cu^{2+}-ZT, panel A) copper is dispersed on the oxide surface, whereas in the case of the Cu_2O-T and Cu_2O-ZT samples the formation of supported Cu_2O particles (with a consequent oxide-oxide interface) is evident.

Table 1. Structure, BET specific surface area and energy gap values of copper-modified TiO_2 and $ZrTiO_4$ based samples.

Sample	Label	Cu loading (%w/w)	Support Structure	B.E.T. Area (m^2 g^{-1})	E_g (eV)
TiO_2	T	-	100 % TiO_2 anatase	65	3.22
Cu^{2+}- TiO_2	Cu^{2+}-T	0.5	100 %TiO_2 anatase	59	3.21
Cu_2O- TiO_2	Cu_2O-T	0.5	100 %TiO_2 anatase	59	3.21
$ZrTiO_4$	ZT	-	100 % $ZrTiO_4$ scrutinyite	62	3.81
Cu^{2+}- $ZrTiO_4$	Cu^{2+}-ZT	0.5	100 % $ZrTiO_4$ scrutinyite	58	3.82
Cu_2O- $ZrTiO_4$	Cu_2O-ZT	0.5	100 % $ZrTiO_4$ scrutinyite	59	3.81

The two procedures of surface modification drastically affect the optical properties of the oxidic supports. Samples Cu^{2+}-T e Cu^{2+}-ZT show pale green and light blue colour respectively, while the Cu_2O-T and Cu_2O-ZT samples show pale pink colour. The UV-Vis reflectance spectra of all modified samples (Fig.1 C and D) show, beside the band gap transition in the UV region, typical of the two supporting oxides, further absorption in the visible region. The two surface impregnated samples (Cu^{2+}-T and Cu^{2+}-ZT, spectra C(c) and D(c) respectively) show two new absorption features, one in the 600-800 nm wavelength range is related to the d-d transition of Cu(II),[19,33] the other shows up in the 400-500 nm range, partially

overlapping the main band gap absorption, and is ascribed to the charge transfer from the valence band (VB) of the oxides to surface Cu(II) species.[8]

The two samples decorated with Cu_2O particles (Cu_2O-T C(b) and Cu_2O-ZT D(b)) show a stronger absorption in the 400-600 nm range with a specific absorption at 475 nm typical of Cu_2O particles.[23,34,35] Also in this case the absorbance in the 600-800 nm region is slightly higher than that of the bare materials. This second feature seems to suggest that, beside the Cu_2O particles, also a small fraction of Cu(II) is present in these two samples.

Table 1 summarizes the main features of the samples employed in this work.

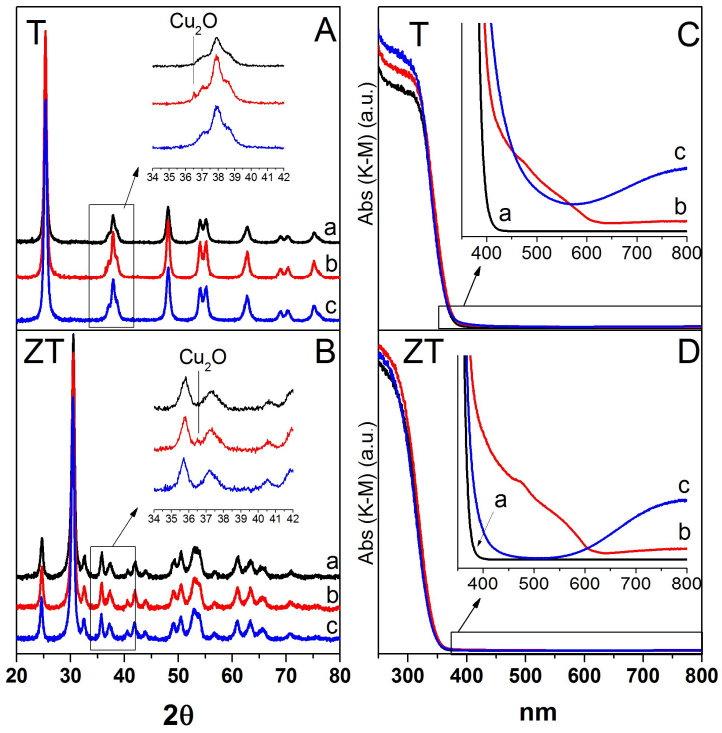

Figure 1. XRD diffractrogams (panel A and B) and DR-UV-Vis spectra (panel C and D) of the bare oxides and the corresponding Cu modified materials. Panel A and C. TiO_2 based materials: a) T, b) Cu_2O-T and c) Cu^{2+}-T. Panel B and D. $ZrTiO_4$ based materials: a) ZT, b) Cu_2O-ZT and c) Cu^{2+}-ZT. The diffraction patterns shown in panel A are due to the anatase polymorph of TiO_2 except for the feature shown in the inset which corresponds to the (111) reflection of cuprite (Cu_2O). The diffraction patterns shown in panel B correspond to the scrutinyite structure ($ZrTiO_4$). Again, the feature highlighted in the inset corresponds to the (111) reflection of cuprite (Cu_2O).

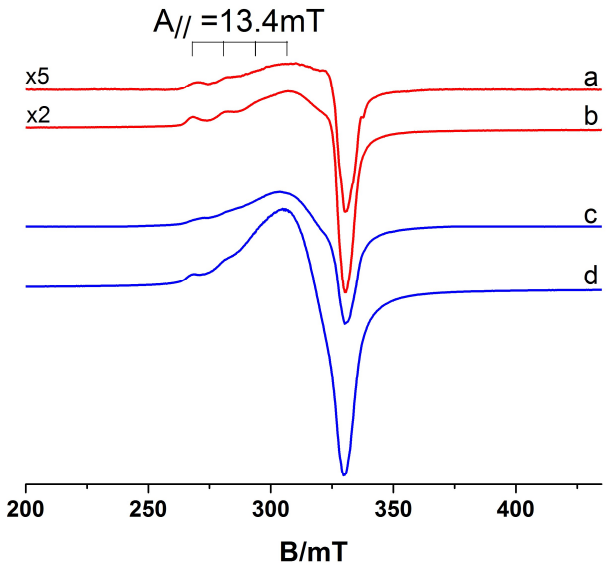

Figure 2. EPR spectra of the Cu modified samples recorded at low temperature under vacuum condition. a) Cu_2O-T, b) Cu_2O-ZT, c) Cu^{2+}-T and d) Cu^{2+}-ZT sample.

Cu^{2+} ions ($3d^9$) bear one unpaired electron and for this reason they can be directly monitored by means of the EPR technique. The EPR spectra of the whole set of as prepared, copper modified samples recorded at 77 K under vacuum are shown in Fig. 2. All samples show EPR signals that appear as the typical fingerprint of Cu^{2+} species. These are much more intense in the case of materials prepared via wet impregnation (Fig. 2c and d). A typical Cu^{2+} signal exhibits an axial **g** tensor splitted in 4 hyperfine lines since the Cu nucleus has nuclear spin I=3/2 and the line multiplicity is $n= 2I +1 = 4$. In all samples the EPR spectrum is characterized by similar spectroscopic features based on the overlap of a broad and asymmetric signal, which dominates the spectrum, with a second one due to a Cu(II) species having partially resolved hyperfine structure in the parallel component ($g_{//}$ = 2.35 and $A_{//}$= 13.4 mT) and non-resolved in the perpendicular one. The first species (broad, unresolved signal) indicates the presence of a family of Cu^{2+} ions mutually interacting with each other via dipolar interaction. The second kind of paramagnetic species is ascribed to isolated Cu(II) ions. Values of the parallel hyperfine coupling constants similar to those found in this case were found also in the case of surface Cu^{2+} species on TiO_2 in an amorphous phase, while in the case of Cu^{2+} incorporated in the TiO_2 matrix the reported A values

are smaller (8-9 mT). [8,9,36] Cu^{2+} ions present in all samples are thus traceable to Cu^{2+} species (isolated or mutually interacting) dispersed on the T and ZT surface, while the presence of CuO bulk is unlikely. Clear evidence of CuO are reported for samples with Cu loading higher than that adopted in this work (0.5%w/w), furthermore the EPR features are certainly not due to CuO but rather to individual Cu^{2+} ionic species. Finally, DR-UV-vis spectra are not compatible with the presence of bulk CuO, which usually shows a continuous absorption in the range UV-vis-NIR.

Peculiar is the fact that in Cu_2O modified samples (Fig. 2 a and b), in principle expected to contain Cu(I) ions only, the presence of Cu(II) ions is also observed. Since the EPR spectrum of bare, unsupported, Cu_2O particles doesn't show any Cu^{2+} signal (data not shown for sake of brevity), it can be inferred that the EPR signals observed for Cu_2O-T and Cu_2O-ZT (Fig. 2a, 2b) samples are not due to Cu^{2+} defects in the original Cu_2O nanoparticles, but, rather to a fraction of the starting Cu(I) ions that is unavoidably oxidized during the preparation procedure and that remains dispersed on the oxide surface.

Combining XRD, DR-UV-Vis and EPR results it can be assumed that the samples prepared by wet impregnation (Cu^{2+}-T, Cu^{2+}-ZT) contain a dispersion of Cu^{2+} ions on the surface of the oxide supports. At variance, the Cu_2O modified samples exhibit, in addition to a small fraction of Cu^{2+} dispersed on the surface of the supporting oxides, Cu_2O particles anchored on the main oxide (T or ZT), thus originating a solid-solid interface (heterojunction).

The electronic structure of the modified starting materials can be preliminarily modelled according to the schemes reported in Fig. 3. Both modification procedures induce the formation of surface isolated Cu^{2+} species (whose reductive potentials are located at +0.16 eV with respect to the H^+/H_2 reduction potential)[8] more abundant in the case of the photocatalysts prepared via wet impregnation. The materials decorated with Cu_2O nanoparticles are additionally characterized by a Cu_2O/oxide heterojunction.

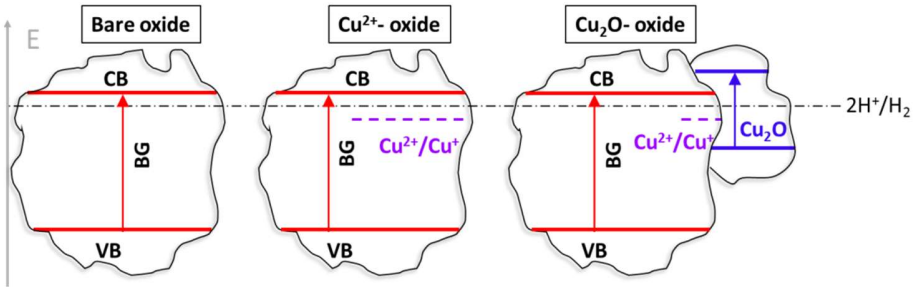

Figure 3. Schematic representation of the band structure alignment of bare and Cu modified samples. The case here reported is that of TiO_2 (T). In the case of zirconium titanate (ZT) the situation is analogous.

3.2. Photocatalytic H_2 evolution test

The basic mechanism involved in H_2 photoproduction in presence of a generic semiconducting oxide can be described by the following steps. First of all, the absorption of photons with energy equal to or larger than the band gap of the semiconductor and the electron-hole pairs formation (eq. 1).

$$OXIDE + h\nu \rightarrow e^-_{(CB)} + h^+_{(VB)} \qquad (1)$$

The photogenerated electrons then reduce the hydrogen according to the following reactions

$$2e^-_{(CB)} + 2H^+ \rightarrow H_2 \qquad (2)$$

$$e^-_{(CB)} + Ti^{4+} \rightarrow Ti^{3+} \qquad (2a)$$

$$2Ti^{3+} + 2H^+ \rightarrow H_2 + 2Ti^{4+} \qquad (2b)$$

Simultaneously photogenerated holes are involved in the oxygen evolution process.

$$2h^+_{(VB)} + H_2O \rightarrow 1/2O_2 + 2H^+ \qquad (3)$$

Even though photoactive oxides like TiO_2 can be photoexcited under band gap irradiation (eq. 1), it is well known the H_2O molecule cannot be efficiently photosplit on bare oxides. For this reason, co-catalyst for both H_2 and O_2 evolution reactions (HER and OER respectively) are usually added to the semiconducting system. In the present case since we were focussed on the role of copper compounds in HER, photocatalytic H_2 evolution was tested irradiating the samples in presence of a 10% v/v methanol aqueous solution, methanol playing the role of sacrificial reactant for oxidation. Adding of a fraction of

this alcohol as a sacrificial agent represents a well-established procedure to scavenge the photogenerated holes so that the one can more easily focus on hydrogen evolution.[4,37] It is worth to mention however that, in this case, a fraction of the photoformed H_2 could derive from the photoreforming of methanol (that competes with the full mineralisation of the alcohol) according to the following reactions:[38,39]

$$CH_3OH \xrightarrow{oxide/h\nu} HCHO + H_2 \qquad (4)$$

$$HCHO + H_2O \xrightarrow{oxide/h\nu} HCO_2H + H_2 \qquad (5)$$

$$HCO_2H \xrightarrow{oxide/h\nu} CO_2 + H_2 \qquad (6)$$

Fig. 4 reports the hydrogen evolution rate curves under UV-Vis irradiation for the whole set of Cu modified photocatalysts compared with the corresponding bare materials. For both oxides, the materials modified with Cu_2O are more active than the materials prepared via wet impregnation which, in turn, show higher activity that the bare materials. For both the bare oxidic matrices (T and ZT) H_2 evolution is basically negligible. The modified TiO_2 samples show higher activity than the corresponding $ZrTiO_4$ samples. With the only exception of Cu_2O-T, which has a high H_2 evolution rate since the beginning of irradiation, all Cu-modified materials show a low rate of H_2 production in the first 30 min. After this time lag (connected to the photoinduced transformation of the materials, see below) the rate of photocatalytic H_2 production increases with a roughly linear trend reaching a plateau in the case of Cu_2O-T only.

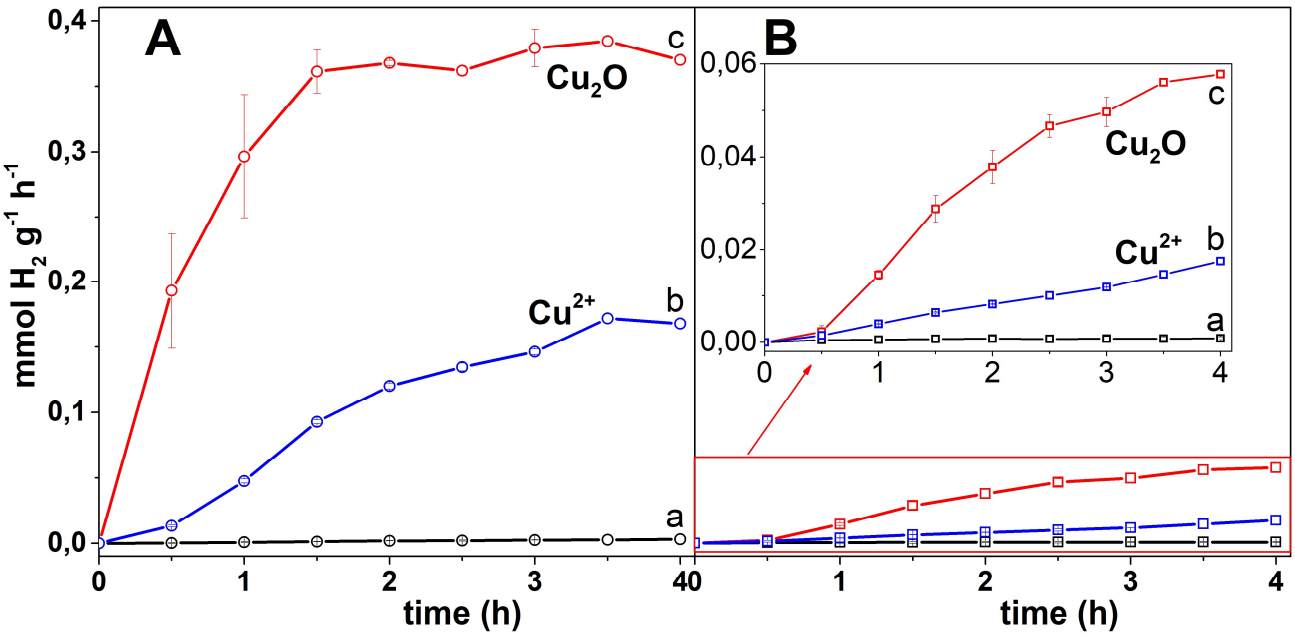

Figure 4. Hydrogen evolution rate (mmol g^{-1} h^{-1}) obtained with (A) TiO_2 based samples; (B) $ZrTiO_4$ based samples. a) bare oxides, b) Cu^{2+}-oxides and c) Cu_2O-oxides.

3.3. Characterization of the photocatalysts under irradiation

3.3.1. EPR characterization at the solid-gas interface

Previous studies have shown that Cu(II) centres in TiO_2 can act as traps for photogenerated electrons and the same behaviour occurs in the photocatalysts investigated in the present work.[14,33,40] Upon UV irradiation in vacuum at 77 K (red spectra in Fig. 5) for the whole set of samples the EPR intensity of the Cu(II) species decreases due to the reduction of the paramagnetic Cu^{2+} centres to diamagnetic forms of copper (Cu^{+}/Cu^{0}). The initial processes can be described as follows:

$$e^{-}_{(CB)} + Cu^{2+} \rightarrow Cu^{+} \qquad (7)$$

In metal oxide the photogenerated holes usually get stabilized on a lattice oxygen producing $O^{\bullet-}$ ions which are, at least in part, EPR detectable.[41] In the present case the relatively weak $O^{\bullet-}$ signal is buried under the Cu^{2+} one which falls in the same spectral region.

It is worthy to note that, by interrupting irradiation (blue spectra in Fig. 5), the behaviour of the two samples modified with cuprous oxide (Cu_2O-T and Cu_2O-ZT, Fig. 5A and C respectively) differs from that of the samples prepared via wet impregnation (Cu^{2+}-T and Cu^{2+}-ZT, Fig. 5B and D respectively). In this second case after interrupting the light, the Cu(II) EPR intensity is fully recovered (indicating that the initial oxidation state is regained due to fast charge recombination) and no new signals are photoformed. In the case of Cu_2O-T and Cu_2O-ZT samples, at variance, the starting intensity of the Cu(II) signal is not fully recovered after light-off and a new weak signal ($g_{average}$= 1.93), more intense in the Cu_2O-T sample, appears. This signal, unambiguously ascribed to Ti^{3+} centres, is originate by electron trapping on Ti^{4+} cations as described by the equation 2a.[42]

Such difference indicates that the effect on charge carriers separation is remarkably different in the two cases and, in the case of Cu_2O modified samples, a longer lifetime of the separated charge carriers is observed. In the case of Cu^{2+}/oxide materials the more abundant Cu^{2+} sites (Fig. 2) act as sink for all photogenerated electrons.

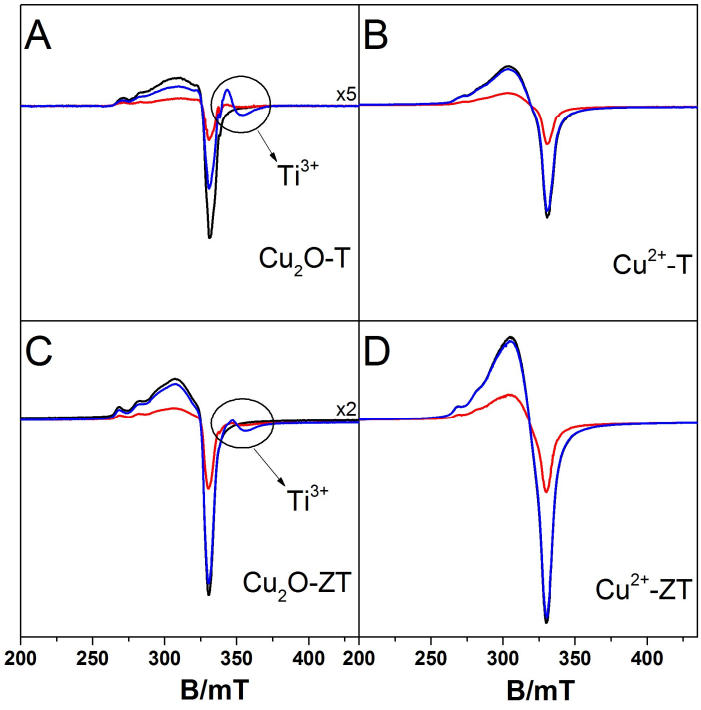

Figure 5. EPR spectra of the as prepared Cu modified samples (black spectra), upon UV-Vis irradition in vacuum at 77 K (red spectra) and after turning off the light (blue spectra). Panel A and C: Cu_2O modified samples. Panel B and D: Cu^{2+}-oxides samples.

3.3.2. EPR characterization at the Solid-Liquid interface

In order to better understand the fate of the charge carriers and the role of the Cu species during H_2 evolution, EPR measurements were performed, at regular intervals, during irradiation of sample suspensions in a 10% v/v methanol/water solution (same condition of the H_2 evolution test). For each measurement the irradiation was stopped and an EPR spectrum was recorded, after each stop, having previously freezed the samples at 77 K in order to block the process and to increase the quality of the spectra. The EPR spectra during H_2 evolution, reported in Fig. 6, represents an EPR picture of the working photocatalysts. Only three spectra (t = 0, 5 and 30 min) are shown for clarity. Inspection of the spectra in Fig. 6 indicates that the presence of Ti^{3+} in conditions of H_2 evolution is much more evident

with respect to the case of vacuum irradiation (Fig. 5). In all cases Ti^{3+} is observed in the spectra and it is the dominant species in TiO_2-based materials (Fig. 6 A, B).

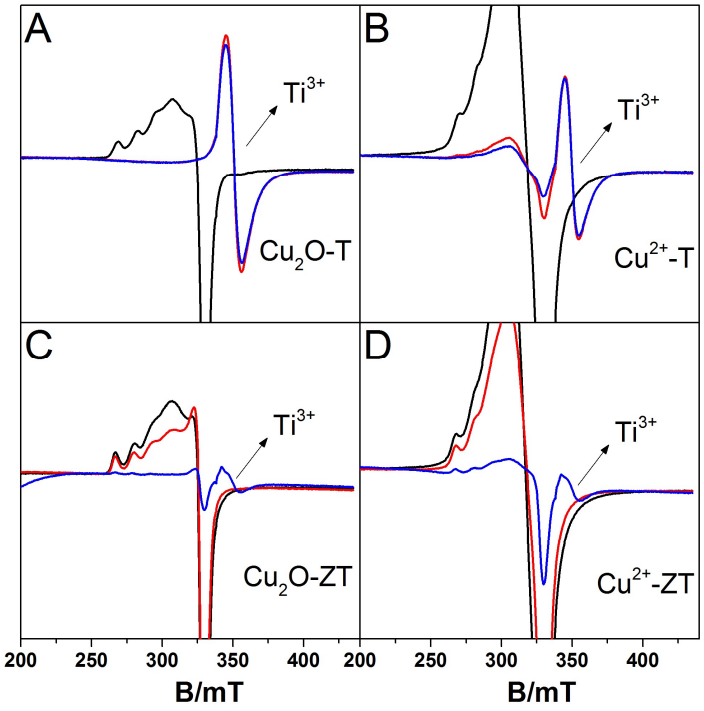

Figure 6. EPR spectra of the suspension of the as prepared Cu modified samples in water-methanol solution (black spectra), after 5 min of UV-Vis irradiation at RT (red spectra) and after 30 min of UV-Vis irradiation at RT (blue spectra). Panel A and C: Cu_2O modified samples. Panel B and D: Cu^{2+}-oxides samples. All the spectra were recorded at 77 K.

Fig. 7 reports the integrated intensities of the EPR signals of the Cu(II) and Ti^{3+} species monitored in the whole experiment (60 min). The first evidence derived from Fig. 6 and Fig. 7 is that the working catalysts is considerably reduced with respect to the starting materials. The concentration of Cu^{2+}, in all cases, drastically decrease (electron trapping, eq. 7) and, though at a different extent for the various samples, Ti^{3+} is formed again by electron trapping.

The deeper extent of photoreduction recorded during H_2 evolution is due, differently from the case of the irradiation under vacuum, to the presence of methanol in the liquid phase, which acts as hole scavenger, enhancing the lifetime of the photoformed electrons. In parallel, inspection of Fig. 6 and Fig. 7 also indicates that, in the case of TiO_2 based samples, after 5 min the Cu(II) species completely disappear in Cu_2O-T, whereas, for Cu^{2+}-T containing more isolated cupric ions (Fig. 2), it reaches a minimum in

intensity. Apart for the concentration of Ti^{3+} ions which is systematically higher in T samples, the intensity trend of the two paramagnetic species (Cu(II) and Ti^{3+}) is similar in the two cases (T, ZT). For both Cu_2O-T and Cu^{2+}-T, Ti^{3+} grows after 5 min irradiation in parallel to the Cu(II) decrease. In the case of the ZT based samples, Ti^{3+} centers show up later when the Cu(II) species tend to their minimum intensity. In the case of Cu_2O-ZT, Ti^{3+} begins to grow up after 10 min of irradiation and for Cu^{2+}-ZT after 20 min of irradiation.

Summarizing, during irradiation in liquid phase during H_2 evolution, the presence of an hole scavenger (CH_3OH) emphasizes the role of photogenerated electrons. The working photocatalysts is rich of trapped electrons that, firstly, reduce Cu^{2+} ions and only later Ti^{4+} cations to Ti^{3+}. In fact, Ti^{3+} centers show up only when the Cu(II) are exhausted or reach a minimum in intensity.

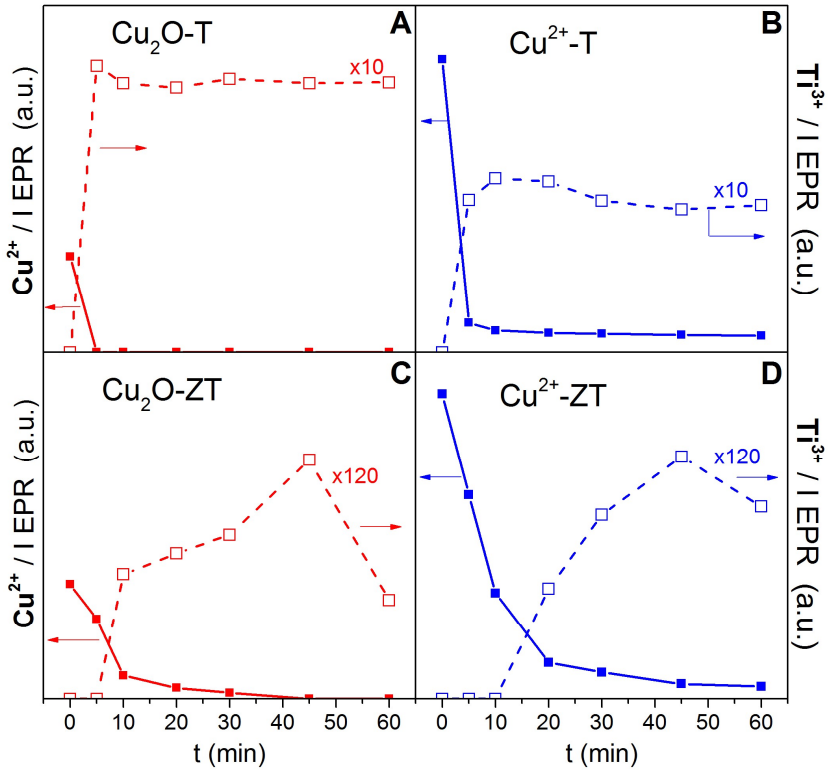

Figure 7. EPR intensities of Cu^{2+} (straight lines) and Ti^{3+} species (dashed lines) at different times of UV-Vis irradiation of Cu_2O-oxides (panels A and C, red lines) and Cu^{2+}-oxides (panels B and D, blue lines) in methanol/water suspension.

3.3.3. DR-UV-Vis characterization at the Solid-Liquid interface

Fig. 8 reports the same experiment shown in Fig. 6 which is, in this case, followed by optical spectroscopy. The effect of irradiation on the oxidic materials (bare and Cu-modified), in the presence of a methanol/water solution (10% v/v), is shown after 30 and 60 min (curves b and c in Fig. 8, curve a refers to the starting material). The presence of the solution causes the onset of two absorption bands, ascribable to the infra-red active groups of the water/methanol solution, centered at about 1000 nm and 1200 nm. which will not be further discussed in the following.

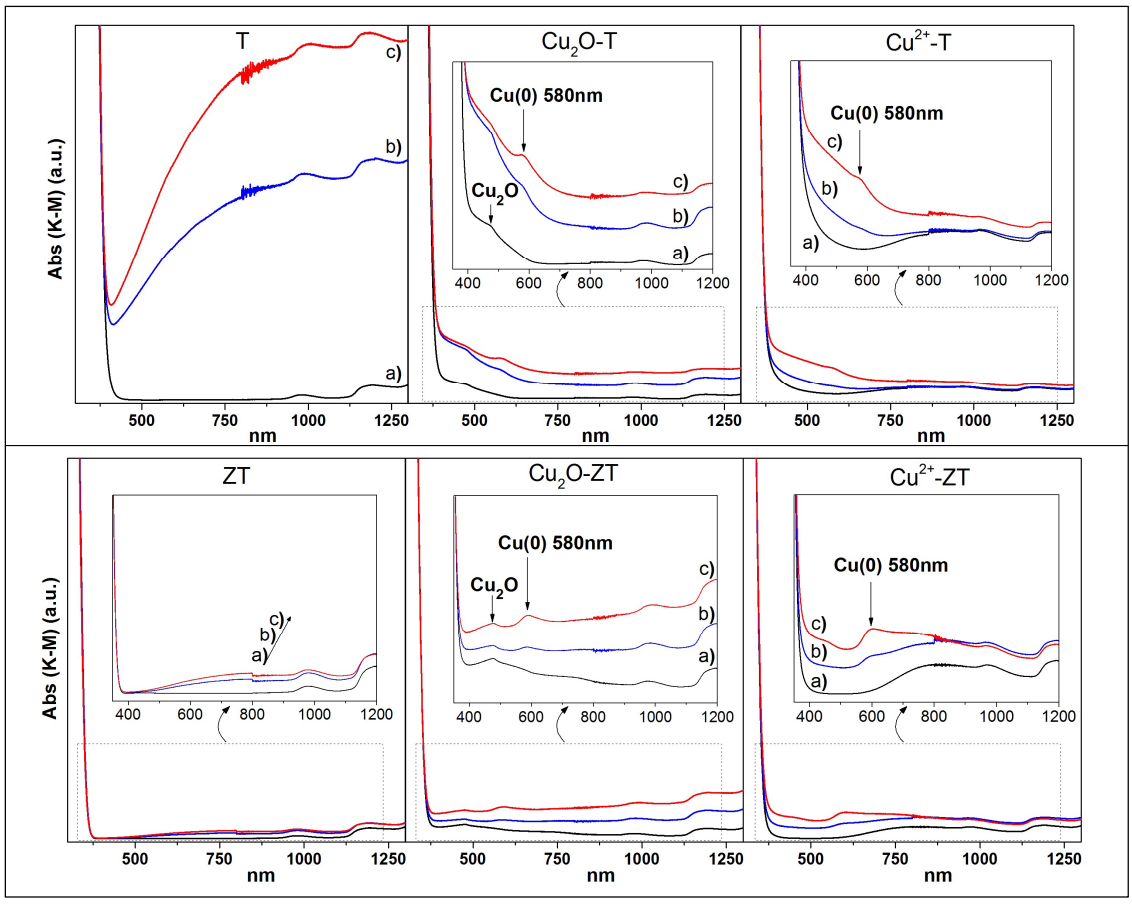

Figure 8. DR-UV-Vis spectra of the different systems in presence of methanol/water solution (10% v/v). a) as prepared samples, b) after 30 min of UV-Vis irradiation and c) after 60 min of UV-Vis irradiation.

As far as the bare materials (T and ZT in Fig. 8) are concerned a continuous absorption in the visible and NIR regions grows along the irradiation process which is due to Ti^{3+} ions formation.[43] Zirconium titanate appears, as already discussed, less reducible than titanium dioxide.[32]

Concerning Cu modified samples the spectra obtained during irradiation are complex due to the presence of copper species in various oxidation states (see Fig. 1). More in detail, in the case of the Cu_2O containing samples (Cu_2O-T and Cu_2O-ZT in Fig. 8) the starting spectroscopic features of the Cu_2O particles, in the region between 400 nm and 600 nm, are preserved after irradiation as indicated by the specific absorption at 475 nm. Simultaneously, after 30 minutes of irradiation, a further absorption peak at about 580 nm clearly appears in both cases. Such feature corresponds to the Surface Plasmonic Resonances (SPR) of metallic copper particles[44,45] and unambiguously indicates that the reduction of the Cu species proceeds up to the zero oxidation state. Since the EPR spectra (Fig. 6 A and C) indicate that the Cu^{2+} species undergo reduction during irradiation, the formation of metallic copper occurs at the expense of Cu^{2+} species dispersed on the surface of the samples. This implies the partial migration of the Cu(II) species through the solution and the subsequent reduction (*vide infra*) or, alternatively, the reduction to Cu(0) and the migration at the surface of these species with consequent aggregation of small metal particles. The latter process is favoured by the reduction to a neutral Cu(0) species not affected by the surface electric fields.

In the case of Cu^{2+}-T and Cu^{2+}-ZT samples, after each irradiation step, a new absorption feature arises in the region between 400 nm and 600 nm similar to that reported for the Cu_2O decorated materials. This feature suggests that the reduction of Cu(II) to Cu(I) occurs.[46] This does not necessarily mean that true Cu_2O particles are formed. The peculiar spectroscopic feature of bulk Cu_2O at 475 nm is, in fact, absent. Most likely the isolated Cu^{2+} species are reduced to similar Cu^{+} ones. Furthermore, it is worth to note that after 60 min of irradiation, also in this case, the formation of metallic copper occurs.

Thus, in Cu_2O containing materials (Cu_2O-T and ZT) metallic copper particles are formed upon irradiation, beside Cu_2O ones. Similar metallic Cu particles are present on the working Cu^{2+} based materials. In this case (Cu^{2+}-T and ZT), however, Cu^+ does not form Cu_2O aggregates but, most likely, remains dispersed at the surface as supported Cu^+ ions.

3.4. Charge carriers dynamics during H_2 evolution reaction

On the basis of the EPR and optical results, a description of both the chemical modifications of the catalysts occurring during irradiation and the hydrogen evolution mechanism can be proposed according to the schemes reported in Fig. 9 and Fig. 10, respectively.

Since the experimental results suggest that the behavior of the ZT based samples is basically the same observed for the T based samples, although overall less effective, in the following the two sets of materials (T and ZT based samples) will be discussed together.

All the investigated Cu-modified samples show, upon UV light irradiation, a higher hydrogen evolution than the corresponding bare materials. The mechanism operating on the two kinds of modified materials is very likely different in the two cases considering the different chemical nature of the copper in the starting samples (mainly Cu(II) in Cu^{2+}-T/ZT and mainly Cu(I) in Cu_2O-T/ZT).

Concerning Cu^{2+} containing samples the EPR characterization shows that Cu^{2+} is easily consumed upon irradiation under vacuum (Fig. 5) and, even more efficiently, in the operative conditions of the photocatalytic reactions (Fig. 6). It is worth to note, furthermore, that Ti^{3+} ions can be photogenerated (eq. 2a) only when the Cu(II) amount is reduced (eq. 7) to a minimum value (Fig. 7). When the photocatalytic reaction reaches a steady state, Cu(II) is absent (Cu_2O-T) or nearly absent in the systems. For this reason, the photocatalytic activity of Cu^{2+}-T/ZT samples in H^+ reduction, has to be ascribed to reduced copper species forming during the irradiation and not to cupric ions. The optical spectroscopy experiments indicate, indeed, that the formation of Cu(0) occurs mainly at the expenses of isolated Cu^{2+}

species which are progressively photoreduced to form, after migration on the surface, small Cu(0) aggregates (see Fig. 9, right-hand side).

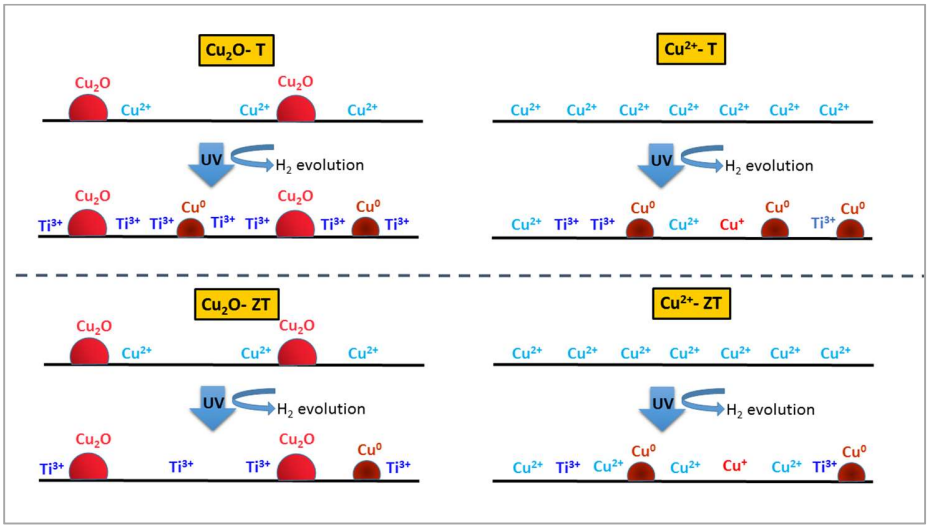

Figure 9. Chemical modifications occurring at the surface of the different Cu modified samples during H_2 evolution reaction.

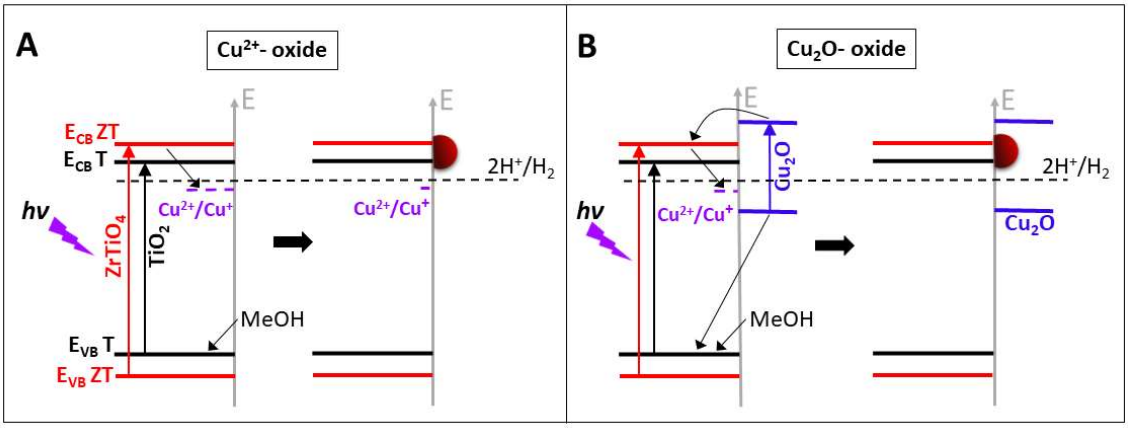

Figure 10. Model of H_2 evolution mechanism occurring on Cu^{2+}-oxides (panel A) and Cu_2O-oxides (panel B) respectively. The band position are reported on the basis of the energy values reported in refs [47,48].

This occurs mainly in the case of Cu^{2+}-T and Cu^{2+}-ZT samples where only dispersed Cu(II) ions are present. The same process however occurs, at a minor extent, on the samples containing Cu_2O particles that show a smaller but non-negligible concentration of dispersed Cu^{2+} ions (Fig. 2).

In the latter case however, the formation of a further small amount of Cu(0) particles at the expenses of Cu_2O ones cannot be excluded. Cu oxides, in fact, can be dissolved in acid solutions to form Cu^{2+}

(leaching), because of the formation of organic acids as a consequence of the partial oxidation of methanol (eq. 5) The formation of acid molecules favour the partial dissolution of copper oxides[49] and the Cu^{2+} ions formed in so far can trap the excited electrons contributing to the formation of a further fraction of metallic Cu, which is deposited on the surface. Notably the Cu nanoparticles formed by photoreduction are only stable in the conditions of the photocatalytic reaction. In fact, along H_2 evolution the original pale colored materials become progressively darker, but exposing the methanol/water suspensions containing the photocatalysts to the atmosphere, they are progressively oxidized recovering the original colour. It is known in fact that copper metallic particle needs protection to avoid chemical corrosion.[25,50] Nevertheless, a fraction of Cu_2O aggregates remains unaffected at the surface, as indicated by the specific absorption at 475 nm (Fig. 8). The Cu^{2+}- and Cu_2O-materials differs therefore, in operative conditions, in terms of the presence of a Cu_2O-oxide interface that is not present in the case of Cu^{2+}-T and Cu^{2+}-ZT systems while Cu(0) particles are present in both cases. This specific composition and the role of Cu_2O are likely the reason of the superior activity of this kind of materials with respect to those prepared by wet impregnation.

The mechanism of H_2 evolution in the described photocatalysts can be tentatively discussed on the basis of the previously illustrated composition of the working systems and also considering the electronic energy of the species involved (Fig. 10). The presence of metallic copper, formed by reduction of Cu^{2+} under irradiation, is the key factor explaining the increased catalytic activity of Cu^{2+}-T and Cu^{2+}-ZT materials with respect to the corresponding bare oxides (Fig. 10A). In these samples Cu(0) represents in fact the dominant Cu species. Metallic copper, contrarily to most prominent Pt or Pd co-catalysts for H_2 photoevolution, is not considered among the best co-catalyst for hydrogen activation, mainly due to the weak Cu affinity for hydrogen chemisorption.[51,52] Nevertheless, metallic copper takes part to important processes such as methanol synthesis from CO and H_2[53,54] and, although further work is necessary for a

full comprehension of the mechanism behind hydrogen photoevolution on Cu(0), several Authors report that metallic Cu can act as a co-catalyst for hydrogen production.[26-29]

In the case of Cu_2O containing materials, which are more active than those based on Cu^{2+}, the superior activity must be due to the maintenance of a fraction of this cuprous oxide phase in working conditions. A plausible mechanism is as follows. Irradiation causes a charge separation in both the Cu_2O particles and the oxidic supports. Because of the relative position of the band potentials, the electrons transfer from the conduction band of Cu_2O to that of the main photocatalytic oxide occurs (Fig. 10B). Simultaneously the photoformed holes in the valence band of T or ZT move to the Cu_2O valence band inhibiting the charge carrier recombination. This mechanism explains the fact that the Ti^{3+} ions formation upon irradiation in vacuum (Fig. 5) is observed in this kind of materials only (Panel A, C) and not in the Cu^{2+} samples (Panel B, D). Summarizing, the synergic effect due to the presence of the Cu_2O/oxide heterojunction and of metallic copper particles leads to a H_2 evolution rate definitely higher than that obtained on Cu^{2+}-T and Cu^{2+}-ZT samples that contain copper metal particles only.

Conclusive remarks.

In this work the photochemistry of copper containing photocatalysts constituted by TiO_2 and $ZrTiO_4$ has been investigated leading to a detailed picture of the composition of the various systems before the reaction and in working conditions. In parallel, the role of the different forms of copper in H_2 evolution reaction has been proposed.

The results obtained via the joint use of EPR and UV-Vis DRS spectroscopies clearly indicate that during the irradiation all the as prepared solids undergo a chemical transformation and metallic copper is generated. Consequently, the real photocatalyst involved in the H_2 evolution reaction is different from the starting material in particular for the photocatalysts prepared via wet impregnation. Furthermore, in the materials decorated with Cu_2O particles, charge carriers separation is more efficient because of the

presence of a Cu_2O/oxide heterojunction which is preserved during the reaction. The better performance in H_2 evolution for this kind of material is essentially due to the presence of the Cu_2O phase. Additionally, a synergic effect caused by the presence of metallic copper particles beside the Cu_2O ones cannot be excluded.

Furthermore, the photoactivity of TiO_2 based materials is systematically higher than that of the $ZrTiO_4$-based ones. This occurs in spite of the more negative potential of the titanate conduction band that in principle should favor H^+ reduction on this photocatalytic oxide. The reason of this behavior has to be searched in the different capability of TiO_2 to stabilize photogenerated electrons (Fig. 6) or, in other words, to be photoreduced. The presence, in working conditions, of a higher concentration of trapped electrons (Ti^{3+}) witnesses a higher capability to limit the recombination of the charge carriers and, therefore, a superior tendency/ability to promote the photocatalytic reduction of hydrogen ions.

AUTHOR INFORMATION

Corresponding Author

* Stefano.livraghi@unito.it

ACKONOWLEDGMENTS

Financial support from the Italian MIUR through the PRIN Project 2015K7FZLH, SMARTNESS “Solar driven chemistry: new materials for photo- and electro-catalysis” is gratefully acknowledged.

REFERENCES

(1) Maeda, K.; Domen, K. Photocatalytic Water Splitting: Recent Progress and Future Challenges. *J. Phys. Chem. Lett.* **2010,** *1* (18), 2655-2661.

(2) Kudo, A.; Miseki, Y. Heterogeneous Photocatalyst Materials for Water Splitting. *Chem. Soc. Rev.* **2009,** *38* (1), 253-278.

(3) Henderson, M. A. A Surface Science Perspective on Photocatalysis. *Surf. Sci. Rep.* **2011,** *66* (6), 185-297.

(4) Chiarello, G. L.; Dozzi, M. V.; Selli, E. TiO_2-Based Materials for Photocatalytic Hydrogen Production. *J. Energy Chem.* **2017,** *26* (2), 250-258.

(5) Li, K.; Chai, B.; Peng, T.; Mao, J.; Zan, L. Preparation of $AgIn_5S_8/TiO_2$ Heterojunction Nanocomposite and its Enhanced Photocatalytic H_2 Production Property under Visible Light. *ACS Catal.* **2013,** *3* (2), 170-177.

(6) Jiang, Z.; Jiang, D.; Yan, Z.; Liu, D.; Qian, K.; Xie, J. A New Visible Light Active Multifunctional Ternary Composite Based on TiO_2–In_2O_3 Nanocrystals Heterojunction Decorated Porous Graphitic Carbon Nitride for Photocatalytic Treatment of Hazardous Pollutant and H_2 Evolution. *Appl. Catal., B* **2015,** *170*, 195-205.

(7) Meng, A.; Zhu, B.; Zhong, B.; Zhang, L.; Cheng, B. Direct Z-Scheme TiO_2/CdS Hierarchical Photocatalyst for Enhanced Photocatalytic H_2-Production Activity. *Appl. Surf. Sci.* **2017,** *442*, 518-527.

(8) Irie, H.; Kamiya, K.; Shibanuma, T.; Miura, S.; Tryk, D. A.; Yokoyama, T.; Hashimoto, K. Visible Light-Sensitive Cu(II)-Grafted TiO_2 Photocatalysts: Activities and X-ray Absorption Fine Structure Analyses. *J. Phys. Chem. C* **2009,** *113* (24), 10761-10766.

(9) Nosaka, Y.; Takahashi, S.; Sakamoto, H.; Nosaka, A. Y. Reaction Mechanism of Cu(II)-Grafted Visible-Light Responsive TiO_2 and WO_3 Photocatalysts Studied by Means of ESR Spectroscopy and Chemiluminescence Photometry. *J. Phys. Chem. C* **2011,** *115* (43), 21283-21290.

(10) Méndez-Medrano, M.; Kowalska, E.; Lehoux, A.; Herissan, A.; Ohtani, B.; Bahena, D.; Briois, V.; Colbeau-Justin, C.; Rodríguez-López, J.; Remita, H. Surface Modification of TiO_2 with Ag Nanoparticles and CuO Nanoclusters for Application in Photocatalysis. *J. Phys. Chem. C* **2016,** *120* (9), 5143-5154.

(11) de Brito, J. F.; Tavella, F.; Genovese, C.; Ampelli, C.; Zanoni, M. V. B.; Centi, G.; Perathoner, S. Role of CuO in the Modification of the Photocatalytic Water Splitting Behavior of TiO_2 Nanotube Thin Films. *Appl. Catal., B* **2018,** *224*, 136-145.

(12) Xu, Y.; Schoonen, M. A. The Absolute Energy Positions of Conduction and Valence Bands of Selected Semiconducting Minerals. *Am. Mineral.* **2000,** *85* (3-4), 543-556.

(13) Barreca, D.; Carraro, G.; Gombac, V.; Gasparotto, A.; Maccato, C.; Fornasiero, P.; Tondello, E. Supported Metal Oxide Nanosystems for Hydrogen Photogeneration: Quo Vadis? *Adv. Funct. Mater.* **2011,** *21* (14), 2611-2623.

(14) Li, G.; Dimitrijevic, N. M.; Chen, L.; Rajh, T.; Gray, K. A. Role of Surface/Interfacial Cu^{2+} Sites in the Photocatalytic Activity of Coupled CuO−TiO_2 Nanocomposites. *J. Phys. Chem. C* **2008,** *112* (48), 19040-19044.

(15) Hou, H.; Shang, M.; Gao, F.; Wang, L.; Liu, Q.; Zheng, J.; Yang, Z.; Yang, W. Highly Efficient Photocatalytic Hydrogen Evolution in Ternary Hybrid TiO_2/CuO/Cu thoroughly Mesoporous Nanofibers. *ACS Appl. Mater. Interfaces* **2016,** *8* (31), 20128-20137.

(16) Chen, W.-T.; Jovic, V.; Sun-Waterhouse, D.; Idriss, H.; Waterhouse, G. I. The Role of CuO in Promoting Photocatalytic Hydrogen Production over TiO_2. *Int. J. Hydrogen Energy* **2013,** *38* (35), 15036-15048.

(17) Artioli, G. A.; Mancini, A.; Barbieri, V. R.; Quattrini, M. C.; Quartarone, E.; Mozzati, M. C.; Drera, G.; Sangaletti, L.; Gombac, V.; Fornasiero, P.; Malavasi, L. Correlation between Deposition Parameters and Hydrogen Production in CuO Nanostructured Thin Films. *Langmuir* **2016,** *32* (6), 1510-1520.

(18) Lalitha, K.; Sadanandam, G.; Kumari, V. D.; Subrahmanyam, M.; Sreedhar, B.; Hebalkar, N. Y. Highly Stabilized and Finely Dispersed Cu_2O/TiO_2: A Promising Visible Sensitive Photocatalyst for Continuous Production of Hydrogen from Glycerol: Water Mixtures. *J. Phys. Chem. C* **2010,** *114* (50), 22181-22189.

(19) Liu, Y. X.; Wang, Z. L.; Huang, W. X. Influences of TiO_2 Phase Structures on the Structures and Photocatalytic Hydrogen Production of CuO_x/TiO_2 Photocatalysts. *Appl. Surf. Sci.* **2016,** *389*, 760-767.

(20) Jung, M.; Scott, J.; Ng, Y. H.; Jiang, Y. J.; Amal, R. CuO_x Dispersion and Reducibility on TiO_2 and its Impact on Photocatalytic Hydrogen Evolution. *Int. J. Hydrogen Energy* **2014,** *39* (24), 12499-12506.
(21) Jung, M.; Hart, J. N.; Scott, J.; Ng, Y. H.; Jiang, Y.; Amal, R. Exploring Cu Oxidation State on TiO_2 and its Transformation During Photocatalytic Hydrogen Evolution. *Appl. Catal., A* **2016,** *521*, 190-201.
(22) Hu, Q. Q.; Huang, J. Q.; Li, G. J.; Chen, J.; Zhang, Z. J.; Deng, Z. H.; Jiang, Y. B.; Guo, W.; Cao, Y. G. Effective Water Splitting using CuO_x/TiO_2 Composite Films: Role of Cu Species and Content in Hydrogen Generation. *Appl. Surf. Sci.* **2016,** *369*, 201-206.
(23) Tamiolakis, I.; Papadas, I. T.; Spyridopoulos, K. C.; Armatas, G. S. Mesoporous Assembled Structures of Cu_2O and TiO_2 Nanoparticles for Highly Efficient Photocatalytic Hydrogen Generation from Water. *RSC Adv.* **2016,** *6* (60), 54848-54855.
(24) Xi, Z. H.; Li, C. J.; Zhang, L.; Xing, M. Y.; Zhang, J. L. Synergistic Effect of Cu_2O/TiO_2 Heterostructure Nanoparticle and its High H_2 Evolution Activity. *Int. J. Hydrogen Energy* **2014,** *39* (12), 6345-6353.
(25) DeSario, P. A.; Pietron, J. J.; Brintlinger, T. H.; McEntee, M.; Parker, J. F.; Baturina, O.; Stroud, R. M.; Rolison, D. R. Oxidation-Stable Plasmonic Copper Nanoparticles in Photocatalytic TiO_2 Nanoarchitectures. *Nanoscale* **2017,** *9* (32), 11720-11729.
(26) Ni, D.; Shen, H.; Li, H.; Ma, Y.; Zhai, T. Synthesis of High Efficient Cu/TiO_2 Photocatalysts by Grinding and their Size-Dependent Photocatalytic Hydrogen Production. *Appl. Surf. Sci.* **2017,** *409* (Supplement C), 241-249.
(27) Montini, T.; Gombac, V.; Sordelli, L.; Delgado, J. J.; Chen, X. W.; Adami, G.; Fornasiero, P. Nanostructured Cu/TiO_2 Photocatalysts for H_2 Production from Ethanol and Glycerol Aqueous Solutions. *ChemCatChem* **2011,** *3* (3), 574-577.
(28) Lv, X. J.; Zhou, S. X.; Zhang, C.; Chang, H. X.; Chen, Y.; Fu, W. F. Synergetic Effect of Cu and Graphene as Cocatalyst on TiO_2 for Enhanced Photocatalytic Hydrogen Evolution from Solar Water Splitting. *J. Mater. Chem.* **2012,** *22* (35), 18542-18549.
(29) Tian, H.; Kang, S.-Z.; Li, X.; Qin, L.; Ji, M.; Mu, J. Fabrication of an Efficient Noble Metal-Free TiO_2-Based Photocatalytic System Using Cu–Ni Bimetallic Deposit as an Active Center of H_2 Evolution from Water. *Sol. Energy Mater. Sol. Cells* **2015,** *134*, 309-317.
(30) Nie, J.; Patrocinio, A. O.; Hamid, S.; Sieland, F.; Sann, J.; Xia, S.; Bahnemann, D. B. W. D.; Schneider, J. New Insights into the Plasmonic Enhancement for Photocatalytic H_2 Production by $Cu\text{-}TiO_2$ upon Visible Light Illumination. *Phys. Chem. Chem. Phys.* **2018,** *20* 5264-5273.
(31) Panarelli, E. G.; Livraghi, S.; Maurelli, S.; Polliotto, V.; Chiesa, M.; Giamello, E. Role of Surface Water Molecules in Stabilizing Trapped Hole Centres in Titanium Dioxide (Anatase) as Monitored by Electron Paramagnetic Resonance. *J. Photochem. Photobiol., A* **2016,** *322-323*, 27-34.
(32) Polliotto, V.; Albanese, E.; Livraghi, S.; Indyka, P.; Sojka, Z.; Pacchioni, G.; Giamello, E. Fifty-Fifty Zr-Ti Solid Solution with a TiO_2-Type Structure: Electronic Structure and Photochemical Properties of Zirconium Titanate $ZrTiO_4$. *J. Phys. Chem. C* **2017,** *121,* (10), 5487-5497.
(33) Dozzi, M. V.; Chiarello, G. L.; Pedroni, M.; Livraghi, S.; Giamello, E.; Selli, E. High Photocatalytic Hydrogen Production on Cu(II) Pre-Grafted Pt/TiO_2. *Appl. Catal., B* **2017,** *209*, 417-428.
(34) Banerjee, S.; Chakravorty, D. Optical Absorption by Nanoparticles of Cu_2O. *Europhys. Lett.* **2000,** *52* (4), 468-473.
(35) Bi, F.; Ehsan, M. F.; Liu, W.; He, T. Visible-Light Photocatalytic Conversion of Carbon Dioxide into Methane Using Cu_2O/TiO_2 Hollow Nanospheres. *Chin. J. Chem* . **2015,** *33* (1), 112-118.
(36) Córdoba, G.; Viniegra, M.; Fierro, J. L. G.; Padilla, J.; Arroyo, R. TPR, ESR, and XPS Study of Cu^{2+} Ions in Sol–Gel-Derived TiO_2. *J. Solid State Chem.* **1998,** *138* (1), 1-6.
(37) Barreca, D.; Fornasiero, P.; Gasparotto, A.; Gombac, V.; Maccato, C.; Montini, T.; Tondello, E. The Potential of Supported Cu_2O and CuO Nanosystems in Photocatalytic H_2 Production. *ChemSusChem* **2009,** *2* (3), 230-233.
(38) Galińska, A.; Walendziewski, J. Photocatalytic Water Splitting over $Pt–TiO_2$ in the Presence of Sacrificial Reagents. *Energy Fuels* **2005,** *19* (3), 1143-1147.

(39) El-Roz, M.; Bazin, P.; Daturi, M.; Thibault-Starzyk, F. On the Mechanism of Methanol Photooxidation to Methylformate and Carbon Dioxide on TiO_2: an Operando-FTIR Study. *Phys. Chem. Chem. Phys.* **2015,** *17* (17), 11277-11283.
(40) Priebe, J. B.; Radnik, J.; Kreyenschulte, C.; Lennox, A. J.; Junge, H.; Beller, M.; Brückner, A. H_2 Generation with (Mixed) Plasmonic Cu/Au-TiO_2 Photocatalysts: Structure–Reactivity Relationships Assessed by in Situ Spectroscopy. *ChemCatChem* **2017,** *9* (6), 1025-1031.
(41) Gionco, C.; Livraghi, S.; Maurelli, S.; Giamello, E.; Tosoni, S.; Di Valentin, C.; Pacchioni, G. Al- and Ga-Doped TiO_2, ZrO_2, and HfO_2: The Nature of O 2p Trapped Holes from a Combined Electron Paramagnetic Resonance (EPR) and Density Functional Theory (DFT) Study. *Chem. Mater.* **2015,** *27* (11), 3936-3945.
(42) Livraghi, S.; Rolando, M.; Maurelli, S.; Chiesa, M.; Paganini, M. C.; Giamello, E. Nature of Reduced States in Titanium Dioxide as Monitored by Electron Paramagnetic Resonance. II: Rutile and Brookite Cases. *J. Phys. Chem. C* **2014,** *118* (38), 22141-22148.
(43) Biedrzycki, J.; Livraghi, S.; Giamello, E.; Agnoli, S.; Granozzi, G. Fluorine- and Niobium-Doped TiO_2: Chemical and Spectroscopic Properties of Polycrystalline n-Type-Doped Anatase. *J. Phys. Chem. C* **2014,** *118* (16), 8462-8473.
(44) Parveen, F.; Sannakki, B.; Mandke, M. V.; Pathan, H. M. Copper Nanoparticles: Synthesis Methods and its Light Harvesting Performance. *Sol. Energy Mater. Sol. Cells* **2016,** *144*, 371-382.
(45) Singh, M.; Sinha, I.; Premkumar, M.; Singh, A. K.; Mandal, R. K. Structural and Surface Plasmon Behavior of Cu Nanoparticles Using Different Stabilizers. *Colloids Surf., A* **2010,** *359* (1), 88-94.
(46) Soroka, I. L.; Shchukarev, A.; Jonsson, M.; Tarakina, N. V.; Korzhavyi, P. A. Cuprous Hydroxide in a Solid Form: Does It Exist? *Dalton Trans.* **2013,** *42* (26), 9585-9594.
(47) Huang, Q.; Kang, F.; Liu, H.; Li, Q.; Xiao, X. D. Highly Aligned Cu_2O/CuO/TiO_2 Core/Shell Nanowire Arrays as Photocathodes for Water Photoelectrolysis. *J. Mater. Chem. A* **2013,** *1* (7), 2418-2425.
(48) Graetzel, M.; Frank, A. J. Interfacial Electron-Transfer Reactions in Colloidal Semiconductor Dispersions. Kinetic Analysis. *J. Phys. Chem.* **1982,** *86* (15), 2964-2967.
(49) Gombac, V.; Sordelli, L.; Montini, T.; Delgado, J. J.; Adamski, A.; Adami, G.; Cargnello, M.; Bernal, S.; Fornasiero, P. CuO_x– TiO_2 Photocatalysts for H_2 Production from Ethanol and Glycerol Solutions. *J. Phys. Chem. A* **2009,** *114* (11), 3916-3925.
(50) Zhang, Z.; Dua, R.; Zhang, L.; Zhu, H.; Zhang, H.; Wang, P. Carbon-Layer-Protected Cuprous Oxide Nanowire Arrays for Efficient Water Reduction. *ACS Nano* **2013,** *7* (2), 1709-1717.
(51) Norskov, J. K.; Bligaard, T.; Logadottir, A.; Kitchin, J. R.; Chen, J. G.; Pandelov, S.; Norskov, J. K. Trends in the Exchange Current for Hydrogen Evolution. *J. Electrochem. Soc.* **2005,** *152* (3), J23-J26.
(52) Alia, S. M.; Pivovar, B. S.; Yan, Y. S. Platinum-Coated Copper Nanowires with High Activity for Hydrogen Oxidation Reaction in Base. *J. Am. Chem. Soc.* **2013,** *135* (36), 13473-13478.
(53) Yang, R. Q.; Yu, X. C.; Zhang, Y.; Li, W. Z.; Tsubaki, N. A New Method of Low-Temperature Methanol Synthesis on Cu/ZnO/Al_2O_3 Catalysts from CO/CO_2/H_2. *Fuel* **2008,** *87* (4-5), 443-450.
(54) Meng, F. Z.; Zhang, Q. D.; Yang, G. H.; Yang, R. Q.; Yoneyama, Y.; Tsubaki, N. Structural and Kinetical Studies on the Supercritical CO_2 dried Cu/ZnO Catalyst for Low-Temperature Methanol Synthesis. *Chem. Eng. J.* **2016,** *295*, 160-166.

TOC

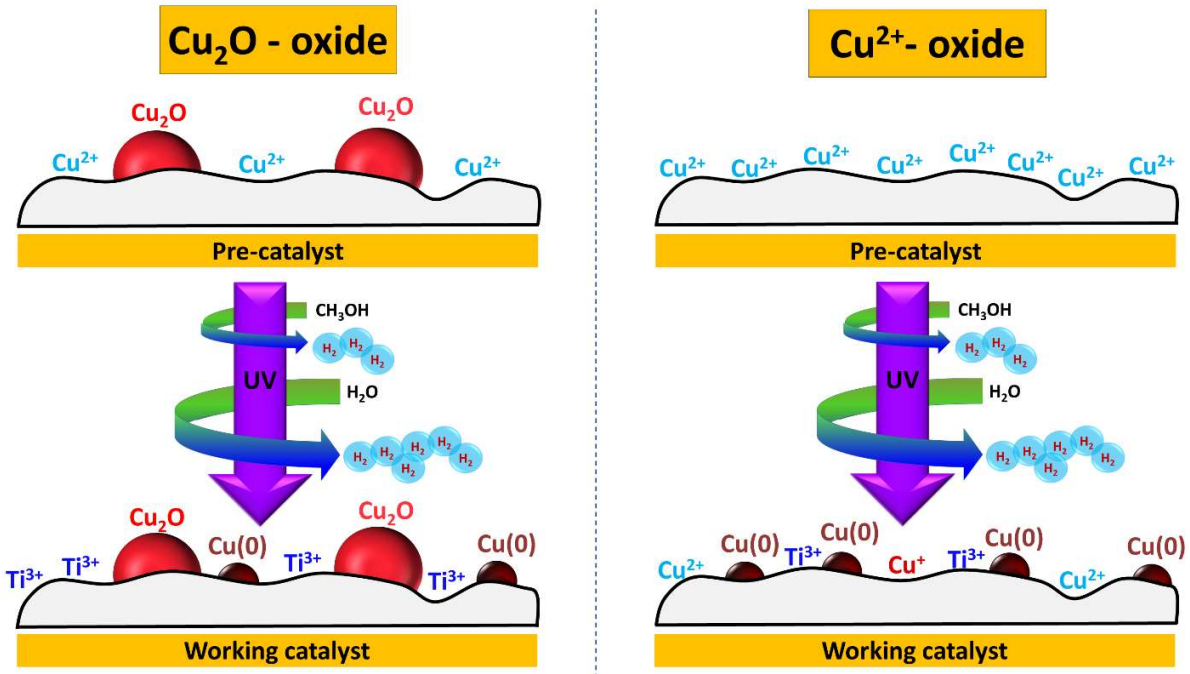
Cu2O - oxide
Cu2+- oxide
Pre-catalyst
Pre-catalyst
UV
UV
CH3OH
H2O
Working catalyst
Working catalyst
Cu(0)
Ti3+
Cu+